

# Density functional theory study of the adsorption of elemental mercury on a 1T-MoS<sub>2</sub> monolayer

Xue-liang MU, Xiang GAO, Hai-tao ZHAO, Mike GEORGE, Tao WU



University of  
**Nottingham**

UK | CHINA | MALAYSIA

University of Nottingham Ningbo China, 199 Taikang East Road, Ningbo,  
315100, China

First published 2018

This work is made available under the terms of the Creative Commons  
Attribution 4.0 International License:

<http://creativecommons.org/licenses/by/4.0>

The work is licenced to the University of Nottingham Ningbo China  
under the Global University Publication Licence:

[https://www.nottingham.edu.cn/en/library/documents/research-  
support/global-university-publications-licence.pdf](https://www.nottingham.edu.cn/en/library/documents/research-support/global-university-publications-licence.pdf)



**University of  
Nottingham**

UK | CHINA | MALAYSIA

# Density functional theory study of the adsorption of elemental mercury on a 1T-MoS<sub>2</sub> monolayer\*

Xue-liang MU<sup>1</sup>, Xiang GAO<sup>2</sup>, Hai-tao ZHAO<sup>1,2</sup>, Mike GEORGE<sup>3</sup>, Tao WU<sup>†‡1</sup>

<sup>(1)</sup>Municipal Key Laboratory of Clean Energy Conversion Technologies, The University of Nottingham Ningbo China, Ningbo 315100, China)

<sup>(2)</sup>College of Energy Engineering, Zhejiang University, Hangzhou 310027, China)

<sup>(3)</sup>School of Chemistry, The University of Nottingham, Nottingham NG7 2RD, UK)

<sup>†</sup>E-mail: tao.wu@nottingham.edu.cn

Received Feb. 13, 2017; Revision accepted Oct. 17, 2017; Crosschecked Dec. 15, 2017

**Abstract:** Elemental mercury has become a global concern because of its significant impact on human health and the ecosystem. A lot of effort has been put towards the removal of elemental mercury from the 2H-MoS<sub>2</sub> (prismatic structure of MoS<sub>2</sub>). However, the mechanism of 1T-MoS<sub>2</sub> (polytype structure of MoS<sub>2</sub>) in Hg<sup>0</sup> capture remains unexplored. In this study, density functional theory (DFT) was adopted to investigate the adsorption mechanism of Hg on a 1T-MoS<sub>2</sub> monolayer. The different possible adsorption positions on the 1T-MoS<sub>2</sub> were examined. For different adsorption configurations, the changes in electronic property were also studied to understand the adsorption process. The results elucidate that chemisorption dominates the adsorption between Hg<sup>0</sup> atoms and the 1T-MoS<sub>2</sub>. It was found that the T<sub>Mo</sub> (on top of the Mo atom) position is the strongest adsorption configuration among all the possible adsorption positions. The adsorption of Hg atoms on the 1T-MoS<sub>2</sub> monolayer is influenced by adjacent S and Mo atoms. The adsorbate Hg<sup>0</sup> atom is found being oxidized on the T<sub>Mo</sub> position of the 1T-MoS<sub>2</sub> with an adsorption energy of 1.091 eV. From the partial density of states (PDOS) analysis of the atoms, the strong interaction between Hg<sup>0</sup> and the 1T-MoS<sub>2</sub> surface is caused by the significant overlap among the d orbitals of the mercury atom and the p orbitals of the S atom and p and d orbitals of the Mo atom.

**Key words:** 1T-MoS<sub>2</sub> monolayer; Mercury capture; Adsorption mechanism; Density functional theory (DFT)

<https://doi.org/10.1631/jzus.A1700079>

**CLC number:** X511/TK09


## 1 Introduction

Elemental mercury (Hg<sup>0</sup>) is the most toxic form of mercury in flue gas released from industrial activity (Galbreath and Zygarlicke, 1996; Presto and Granite, 2006). Because it is insoluble in water, highly volatile, and chemically inert, it can be trans-

ported in air over long distances and periods of time (Gao *et al.*, 2013; Lim and Wilcox, 2013). Once it returns to the biosphere, mercury can bio-accumulate in the ecosystem and become a major threat to human health (UNEP, 2013a; 2013b; Liang *et al.*, 2015). As a consequence, since 1990 a series of policies and legislation on mercury control has been published to prevent the further invasion of mercury, such as Clean Air Act Amendments (1990) (Johansen 2003), Mercury and Air Toxics Standards (MATS) (2011) (EPA, 2011), the Minamata Convention (2013) (UNEP, 2013c). Driven by a series of policies, mercury emissions in Canada, for example, were reduced from about 33 t to 6 t per annum between 1990 and 2000 (UNEP, 2002). Nowadays, more stringent emission legislation has been introduced by many regions

<sup>‡</sup> Corresponding author

\* Project supported by the National Key R&D Program of China (2017YFB0603202), the Ningbo Natural Science Foundation (No. 2017A610060), the National Natural Science Foundation of China (No. 51706114), and the China Postdoctoral Science Foundation (No. 2016M601942)

 ORCID: 0000-0001-6469-9613

© Zhejiang University and Springer-Verlag GmbH Germany, part of Springer Nature 2018

worldwide (Jones, 1999; Praveen, 2003). There is therefore an urgent need for the development of new materials for the control of airborne mercury.

Our previous research showed that MoS<sub>2</sub> is an elemental Hg trapping agent with a trigonal prismatic (2H) structure (Zhao *et al.*, 2016), wherein the layer of Mo atoms is sandwiched between two layers of S atoms, such that each Mo is coordinated to six S atoms in a trigonal prismatic geometry (Yin *et al.*, 2011; Chhowalla *et al.*, 2013). Experimental and theoretical studies have demonstrated that MoS<sub>2</sub>, a type of graphene-like 2D material, is an excellent Hg adsorbent (Zhao *et al.*, 2016). In our previous research, the 2H-MoS<sub>2</sub>, the most stable phase of a MoS<sub>2</sub> monolayer, has been examined extensively for the adsorption of mercury on the defect-free to defective surface. However, not much work has been carried out on the adsorption of mercury on the other geometric structure of MoS<sub>2</sub>, the polytype (1T) with a tetragonal symmetry, which has one MoS<sub>2</sub> layer per repeat unit in the octahedral phase.

The 1T-MoS<sub>2</sub> monolayer is a metastable phase of MoS<sub>2</sub>, and this has attracted attention because of its unique properties since it was fabricated for the first time (Wypych and Schollhorn, 1992) and a series of techniques has been developed to characterize the structure of 1T-MoS<sub>2</sub> (Wypych *et al.*, 1998). Compared with 2H-MoS<sub>2</sub>, the metastable phase has a metallic character, and as such, may provide significantly improved catalytic activity compared with its 2H counterpart. Furthermore, one pronounced property of mercury is its affinity to other metals, such as gold, silver, and copper (Aboud *et al.*, 2008). It was reported that Hg<sup>0</sup> atoms can easily bind to sulfurized adsorbents (Asasian and Kaghazchi, 2015). It was also found that the 1T phase could replace noble metals, such as Pt in hydrodesulfurization reactions and hydrogen evolution reaction (HER) processes (Putungan and Kuo, 2014). Therefore, to better understand the potential of MoS<sub>2</sub> in mercury capture, in addition to the understanding of mercury adsorption on 2H-MoS<sub>2</sub>, it is essential to examine the adsorption of mercury on the 1T-MoS<sub>2</sub>.

Because of the metallic structure of the 1T-MoS<sub>2</sub>, the 1T phase can transform to the 2H phase at a temperature in the range of around 100–300 °C (Goki *et al.*, 2012). Although there is still no clear consensus on the optimum structural phase transition

temperature, there is still a lot of work being carried out on the stabilization of the metallic structure (Gao *et al.*, 2015). However, very little has been done on the adsorption properties of the metallic 1T phase of MoS<sub>2</sub>, especially the 1T phase of MoS<sub>2</sub> material for the adsorption of elemental Hg. In this study, the possible configurations for the adsorption of Hg atoms on the 1T-MoS<sub>2</sub> were examined by density-functional theory (DFT) modelling. The partial density of states (PDOS) and charge transfer for the most stable configuration were studied in detail to show the mechanism of mercury adsorption on the 1T-MoS<sub>2</sub> surface.

In the calculation, although *ab initio* methods such as DFT have been proposed to point out weak interactions, the main difficulty is that weak interactions are long-range. In addition, commonly used approximations such as the local-density approximation (LDA) are suitable for short range and are not appropriate for these long-range interactions. In this simulation work, the overlap of electronic densities around each atom is the basis of all calculation and when this overlap is estimated to be too small, it is not possible to get an accurate result for the system. Therefore, to overcome this problem, a semi-empirical  $r^{-6}$  term such as density functional theory-dispersion correction (DFT-D) is adopted (Sato and Nakai, 2009; Hasnip *et al.*, 2014). Because of the great precision and efficiency of simulations of localized d and 2p orbital with plane-waves basis sets, ultrasoft pseudo-potentials (USPPs) are employed in first-row and transition-metal systems (Vanderbilt, 1990).

## 2 Methodology

Simulation in this study was conducted using the exchange-correlation functional GGA-PW91-OBS. The DFT-D takes into account the charge of the dispersion forces (Ortmann *et al.*, 2006), as conducted by the CASTEP package (Clark *et al.*, 2005). USPPs were applied to all ion-electron interactions in the system (Vanderbilt, 1990). The valence configurations of Mo, S, and Hg atoms were 4p<sup>6</sup>4d<sup>5</sup>5s<sup>1</sup>, 3s<sup>2</sup>3p<sup>4</sup>, 5d<sup>10</sup>6s<sup>2</sup>, respectively. To ensure convergence, convergence with respect to both energy cutoff and *k*-point mesh was set as fine quality (an energy cutoff

of 310 eV and  $2 \times 2 \times 1$   $k$ -points mesh). The total energy of the 1T-MoS<sub>2</sub> ( $4 \times 4$ ) was converged to within  $1 \times 10^{-5}$  eV/atom using the method of Monkhorst-Pack (Chadi, 1977). In addition, the self-consistent field (SCF) calculation was kept within the energy convergence criterion of  $1 \times 10^{-6}$  eV/atom and a smearing width of 0.1 eV was used for the treatment of the metallic system. For supercell calculations, the same modeling parameters were applied.

Since all atomic layers are relaxed in the 1T-MoS<sub>2</sub> ( $4 \times 4$ ) (Liu *et al.*, 2010), to search for the most-stable configuration of the 1T-MoS<sub>2</sub> monolayer and the Hg atoms, the total energy minimization method introduced by Broyden Fletcher Goldfarb Shanno (BFGS) was adopted in this study (Pfrommer *et al.*, 1997). The total-energy difference was set to be within  $10^{-5}$  eV/atom, and the maximum force was set to be within 0.03 eV/Å, while the maximum stress was set to be within 0.05 GPa and the maximum atom displacement was set to be within 0.001 Å. For the interactions among periodical slabs, a vacuum region of 25 Å was also applied in the direction perpendicular to the 1T-MoS<sub>2</sub> plane. The isolated Hg atom was calculated in a  $(10 \text{ Å})^3$  supercell.

The adsorption energy equation ( $E_{\text{ads}}$ ) was determined as

$$E_{\text{ads}} = E_{\text{Hg+1T-MoS}_2} - (E_{\text{Hg}} + E_{\text{1T-MoS}_2}), \quad (1)$$

where  $E_{\text{ads}}$  is the ground state energy of the free Hg<sup>0</sup> atom;  $E_{\text{1T-MoS}_2}$  is the total energy of the 1T-MoS<sub>2</sub> monolayer, and  $E_{\text{Hg+1T-MoS}_2}$  is the total energy of the Hg<sup>0</sup>-1T-MoS<sub>2</sub> slab of the stable adsorption configuration. By definition, a more negative adsorption energy suggests a more favorable exothermic Hg adsorption on the 1T-MoS<sub>2</sub> surface.

### 3 Results and discussion

#### 3.1 Geometric structure

The positions of all atoms were fully relaxed in the 1T-MoS<sub>2</sub> monolayer to ensure the accuracy of the results. As shown in Fig. 1, the pristine structure of the 1T-MoS<sub>2</sub> monolayer is relaxed with the optimized unit cell (lattice constant  $a=b=3.166$  Å), which is close to the result ( $a=3.169$  Å) reported by other re-

searchers (Enyashin and Seifert, 2012). There are four possible adsorption positions of an Hg<sup>0</sup> atom on the 1T-MoS<sub>2</sub> monolayer: (1) on top of a Mo atom ( $T_{\text{Mo}}$ ); (2) on top of the space between neighboring S and Mo atoms ( $B_{\text{Mo-S}}$ ); (3) on top of an S atom of the top sulphur plane ( $TT_{\text{S}}$ ); and (4) on top of an S atom on the bottom sulphur plane ( $TB_{\text{S}}$ ), and these are shown in Fig. 2a–d respectively after the optimization of the adsorption configuration. It is shown that the Hg<sup>0</sup> atom is favorably adsorbed at the  $T_{\text{Mo}}$  adsorption position with the highest adsorption energy of  $-1.091$  eV, which is the site that was also found as the best site for the adsorption of other transition metals on 2H-MoS<sub>2</sub>, such as Fe, Co, and Ni. (Huang *et al.*, 2013). It is also observed in this study that the Hg atom is not adsorbed at the position right on top of a Mo atom but with a deviation from Mo atom along the Mo-S bond, as illustrated in Fig. 2a. This is common in the adsorption position of  $B_{\text{Mo-S}}$  and  $TB_{\text{S}}$ . Under the influence of the Hg atoms adsorbed, the structures of the four adsorption positions on the 1T-MoS<sub>2</sub> monolayer are deformed. It suggests that the geometric structure of pristine 1T-MoS<sub>2</sub> is unstable and is easily affected by external interference.

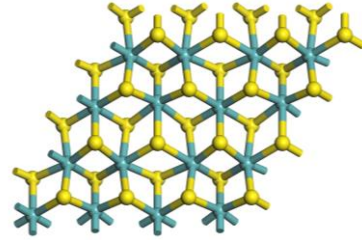


**Fig. 1 Optimized structure of clean 1T-MoS<sub>2</sub> monolayer (yellow atom is S atom, and aquamarine atom is Mo atom)**

Note: for interpretation of the references to color in this figure legend, the reader is referred to the web version of this article

#### 3.2 Adsorption energy

The results of DFT-D and DFT methods are listed in Table 1. Because the DFT-D mainly focuses on the dispersion force between adsorbent and the adsorbate system, the adsorption behavior of a single Hg atom can be calculated more accurately. Therefore, the following discussion is mainly focused around DFT-D methods. Based on Eq. (1), the stability of the adsorption configurations is found to be of the order of  $T_{\text{Mo}} > B_{\text{Mo-S}} > TT_{\text{S}} > TB_{\text{S}}$ , as shown in Table 1. All the four stable adsorption positions show

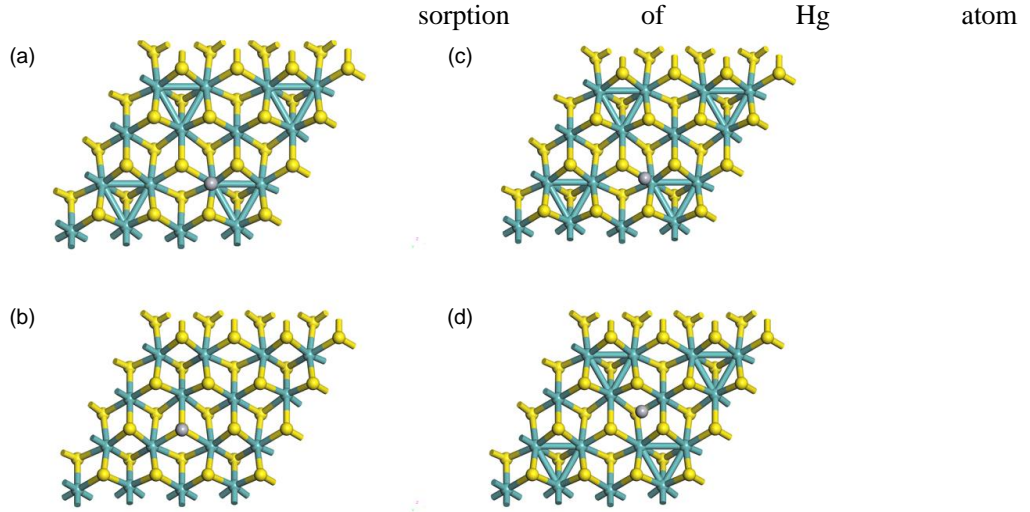


**Fig. 2 Optimized stable structure of 1T-MoS<sub>2</sub> monolayer with adsorbed Hg atom**

(a) Hg atom adsorbed on the top site of a Mo atom ( $T_{Mo}$ ); (b) Hg atom adsorbed on the top site of the bridge site between a S-Mo bond ( $B_{Mo-S}$ ); (c) Hg atom adsorbed on the top site of a S atom in top Sulphur plane ( $TT_S$ ); (d) Hg atom adsorbed on the top site of a S atom in bottom Sulphur plane ( $TB_S$ ) (yellow atom is S atom, and aquamarine atom is Mo atom)

Note: for interpretation of the references to color in this figure legend, the reader is referred to the web version of this article

**Table 1 Adsorption properties of Hg<sup>0</sup> atom on stable adsorption configuration of 1T-MoS<sub>2</sub> monolayer with DFT-D and DFT methods**

Position	$E_{ad}$ (eV)		Frequency (cm <sup>-1</sup> ) <sup>1</sup>		$d_{(Hg-NA S)}$ (Å) <sup>2</sup>		$d_{(Hg-NA Mo)}$ (Å) <sup>3</sup>	
	DFT-D	DFT	DFT-D	DFT	DFT-D	DFT	DFT-D	DFT
$T_{Mo}$	-1.091	-0.982	949.653	3767.507	3.653	3.755	4.822	5.039
$B_{Mo-S}$	-1.085	-0.455	3579.327	6110.059	3.763	3.862	4.856	5.241
$TT_S$	-1.074	-0.967	2686.095	1668.000	3.767	3.910	5.525	5.831
$TB_S$	-1.067	-0.583	1996.348	4164.766	3.771	3.934	5.287	5.447

Note: 1: optimized geometry of final frequency; 2: optimized distance between Hg and the nearest adjacent (NA) S atom; 3: optimized distance between Hg and NA Mo atom

sufficient adsorption energy to allow the Hg atoms to be chemically adsorbed on the 1T-MoS<sub>2</sub> monolayer (Atkins, 2001). Comparing Figs. 2a, 2b and 2c, it can be seen that for the stable adsorption positions with Hg atoms adsorbed, the Hg atom is initially adsorbed at the positions of  $T_{Mo}$ ,  $B_{Mo-S}$ , and  $TB_S$ , but eventually deviated along the bond of Mo and S atoms. However, the adsorption position of  $T_{Mo}$  is very close to the Mo atom with the shortest distance between the Hg and the nearest adjacent (NA) Mo atom (4.822 Å). Furthermore, the distance between the Hg atom and the NA Mo/S atom is the shortest among the four potential adsorption sites. That means the Mo atoms of the 1T-MoS<sub>2</sub> monolayer may affect the behavior of Hg adsorption. The adsorption site of  $TT_S$  shows a shorter distance between the Hg atom and the NA S atom than that of the  $TB_S$ , which means that the ad-

on the 1T-MoS<sub>2</sub> monolayer is also possibly contributed to by the NA S atoms in the top sulphur plane.

### 3.3 Electronic structure

The adsorption mechanism is mainly determined by the change of electronic structure in the Hg-1T-MoS<sub>2</sub> slab. The charge transfer of all atoms and the relevant PDOS analysis were conducted in this study. Hirshfeld charge analysis is based on the variation of density of the free atomic electron density (Delley, 1986). The atomic charges for the pristine 1T-MoS<sub>2</sub> monolayer, the free Hg atom, and the Hg-1T-MoS<sub>2</sub> slab were calculated by the Hirshfeld method. The charge transfer is in accordance with the difference of the electron state in each individual atom before and after adsorption (Table 2), the atomic

indices of which are labeled in Fig. 3. A positive value of charge transfer

**Table 2 Hirshfeld charge analysis for different adsorption positions on 1T-MoS<sub>2</sub>**

Position	Charge analysis (eV)				
	Atomic index	After adsorption	Before adsorption	Charge transfer	
T <sub>Mo</sub>	S(2)	-0.1	-0.11	-0.01	
	S(4)	-0.1	-0.11	-0.01	
	S(8)	-0.11	-0.1	0.01	
	S(12)	-0.1	-0.11	-0.01	
	S(20)	-0.11	-0.1	0.01	
	S(21)	-0.1	-0.09	0.01	
	S(29)	-0.1	-0.09	0.01	
	S(31)	-0.1	-0.09	0.01	
	Mo(8)	0.21	0.2	-0.01	
	Mo(9)	0.21	0.2	-0.01	
	Mo(11)	0.21	0.2	-0.01	
	Mo(12)	0.21	0.2	-0.01	
	Mo(16)	0.21	0.2	-0.01	
	Hg	0.04	0	-0.04	
B <sub>Mo-S</sub>	S(2)	-0.1	-0.11	-0.01	
	S(4)	-0.1	-0.11	-0.01	
	S(8)	-0.11	-0.1	0.01	
	S(12)	-0.1	-0.11	-0.01	
	S(20)	-0.11	-0.1	0.01	
	S(21)	-0.1	-0.09	0.01	
	S(29)	-0.1	-0.09	0.01	
	S(31)	-0.1	-0.09	0.01	
	Mo(11)	0.21	0.2	-0.01	
	Mo(12)	0.21	0.2	-0.01	
	Mo(16)	0.21	0.2	-0.01	
	Hg	0.03	0	-0.03	
	TB <sub>S</sub>	S(4)	-0.1	-0.11	-0.01
		S(8)	-0.11	-0.1	0.01
S(11)		-0.1	-0.09	0.01	
S(20)		-0.11	-0.1	0.01	
S(21)		-0.1	-0.09	0.01	
S(24)		-0.1	-0.11	-0.01	
S(31)		-0.1	-0.09	0.01	
Mo(1)		0.21	0.2	-0.01	
Mo(6)		0.21	0.2	-0.01	
Mo(11)		0.21	0.2	-0.01	
Mo(16)		0.21	0.2	-0.01	
Hg		0.02	0	-0.02	
TT <sub>S</sub>		S(8)	-0.11	-0.1	0.01
		Mo(3)	0.21	0.2	-0.01
	Mo(4)	0.21	0.2	-0.01	
	Mo(8)	0.21	0.2	-0.01	
	Hg	0.01	0	-0.01	

Note: the missing atom index means no charge transfer before and after adsorption, the results unit is eV

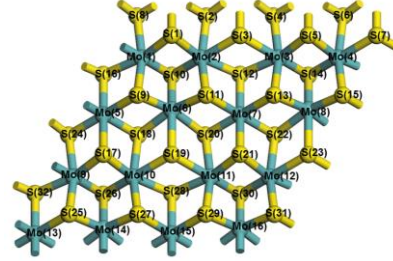


**Fig. 3 Atomic indices for 1T-MoS<sub>2</sub> monolayer (yellow atom is S atom, aquamarine atom is Mo atom)**

Note: for interpretation of the references to color in this figure legend, the reader is referred to the web version of this article means the atom gains electrons after adsorption, while a negative value of that means the atom donates electrons after adsorption.

As shown in Table 2, the order of the Hg charge transfer is recognized as T<sub>Mo</sub>>B<sub>Mo-S</sub>>TB<sub>S</sub>>TT<sub>S</sub>, which is in a similar order to that of the stability of the four adsorption configurations, except for the TB<sub>S</sub> and TT<sub>S</sub> positions. The Hg atom adsorbed on the T<sub>Mo</sub> adsorption site has the largest charge transfer of -0.04 eV after adsorption, while the Hg atoms on the other three potential adsorption positions donate different electrons to the 1T-MoS<sub>2</sub> monolayer. It indicates that the Hg is oxidized after it is adsorbed on the 1T-MoS<sub>2</sub> monolayer. For the four stable adsorption configurations, the Mo atoms have negative charge transfer (-0.01 eV) in those different potential adsorption positions. It is worth noting that the T<sub>Mo</sub> adsorption site has the most Mo atoms, i.e. Mo (8), Mo (9), Mo (11), Mo (12), Mo (16), that participate in the adsorption process. As for the T<sub>Mo</sub> adsorption position, the S atoms in the top S plane, i.e. S(21), S(29) and S(31), show positive charge transfer (0.01 eV) in the Hg-1T-MoS<sub>2</sub> monolayer system. In addition, the S atoms in the bottom S plane, i.e. S(2), S(4) and S(20), also show negative charge transfer (-0.01 eV) in the Hg-1T-MoS<sub>2</sub> monolayer system. Consequently, the oxidized Hg atoms with positive charge are bonded with S atoms in the top S plane that accept electrons from neighboring Mo atoms, the Hg atoms, and the S atoms in the bottom S plane. Hence, the adsorption of Hg at the T<sub>Mo</sub> position is very stable.

To further understand the electronic interactions of the adsorbate Hg atom with the 1T-MoS<sub>2</sub> monolayer at the T<sub>Mo</sub> adsorption site, the density of state (DOS) of the system was investigated by analyzing

the electron change of each individual orbital and the energy levels. There are obvious changes for orbitals

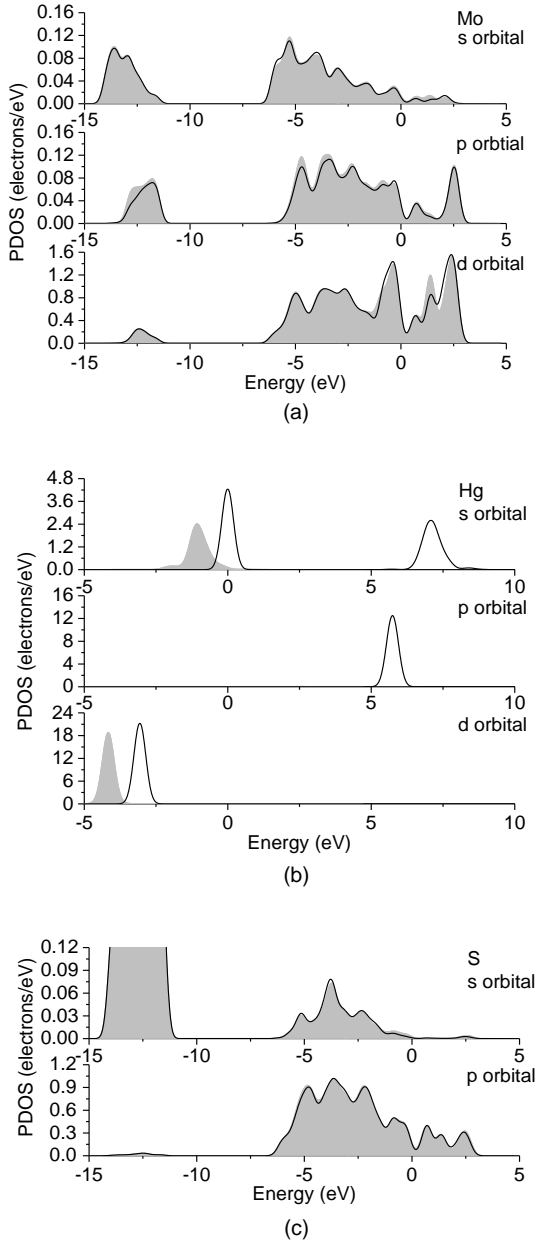


**Fig. 4** PDOS analysis for Hg atom and adjacent Mo and S atoms on  $T_{Mo}$  position of 1T-MoS<sub>2</sub> monolayer: (a) PDOS of s, p and d orbitals for Mo atom; (b) PDOS of s, p, and d orbitals for isolated Hg atom; (c) PDOS of s and p orbitals for S atom (black line means before adsorption, the grey shadow means after adsorption)

Note: for interpretation of the references to color in this figure legend, the reader is referred to the web version of this article

of the Hg, Mo, and S atoms at the PDOS and energy level, as shown in Fig. 4. The PDOS peaks of d, s, and

p orbitals of an isolated Hg<sup>0</sup> atom are approximately -3.1, 0 and 5.7 eV before adsorption, respectively. However, after adsorption, all the PDOS peaks of the Hg atom shift left while the state of the s and p orbitals significantly decrease in energy level. All these changes confirm that strong interactions occur between Hg<sup>0</sup> and the 1T-MoS<sub>2</sub> monolayer. The orbitals of the NA Mo atom and the NA S atom were analyzed to show possible co-interaction with the Hg atom. As illustrated in Figs. 4a and 4c, the s, p and d orbitals of the NA Mo atom and the s and p orbitals of the S atom change slightly after adsorption. In particular, the p orbitals of the NA Mo atom and of the NA S atom become higher in PDOS value and overlap with the s and d orbitals of the Hg atom. It indicates the bonding of s orbital of the Hg atom and p orbitals of the S atom. The d orbitals of the Hg atom interact with the p and d orbitals of the Mo atom and the s orbital of the S atom strongly. It therefore suggests that there are strong interactions between the 1T-MoS<sub>2</sub> monolayer and the adsorbate Hg atoms. It can also be concluded that the 1T-MoS<sub>2</sub> monolayer can oxidize the adsorbate Hg atoms. Both the chemisorption and the oxidation ability of the 1T-MoS<sub>2</sub> monolayer contribute to its good performance in Hg adsorption.

## 4 Conclusions

The DFT modelling of the adsorption of Hg<sup>0</sup> atom on the 1T-MoS<sub>2</sub> monolayer showed that the Hg atoms are favorably adsorbed on the  $T_{Mo}$  of the 1T-MoS<sub>2</sub> slab with an adsorption energy of 1.091 eV. The most stable adsorption configuration in the Hg-1T-MoS<sub>2</sub> slab is chemisorption. The PDOS and charge transfer analyses also show that the Hg atoms adsorbed on the  $T_{Mo}$  position are oxidized and interact with the 1T-MoS<sub>2</sub> slab strongly with a number of Mo atoms and S atoms from both the top and bottom S planes participating in the adsorption. It is evident in this study that the 1T-MoS<sub>2</sub> is an excellent adsorbent for Hg<sup>0</sup> capture.

## Acknowledgements

This project is partially sponsored by the National Key R&D Program of China (2017YFB0603202), the Ningbo Natural Science Foundation (No. 2017A610060), the National Natural Science Foundation of China (No. 51706114), and the China Postdoctoral Science Foundation (No. 2016M601942) The University of Nottingham Ningbo China is acknowledged for the provision of a full scholarship



to the first author.

## References

- About S, Sasmaz E, Wilcox J, 2008. Mercury adsorption on PdAu, PdAg and PdCu alloys. *Main Group Chemistry*, 7:205-215.  
<http://dx.doi.org/10.1080/10241220802465213>
- Asasian N, Kaghazchi T, 2015. Sulfurized activated carbons and their mercury adsorption/desorption behavior in aqueous phase. *International Journal of Environmental Science and Technology*, 12:2511-2522.  
<http://dx.doi.org/10.1007/s13762-015-0818-x>
- Atkins PW, 2001. *Physical Chemistry*. Oxford University Press.
- Chadi DJ, 1977. Special point for Brillouin-zone integrations. *Physical Review B*, 13:5188-5192.
- Chhowalla M, Shin HS, Eda G, et al., 2013. The chemistry of two-dimensional layered transition metal dichalcogenide nanosheets. *Nature Chemistry*, 5:263-275.  
<http://dx.doi.org/10.1038/nchem.1589>
- Clark SJ, Segall MD, Pickard CJ, et al., 2005. First principles methods using CASTEP. *Zeitschrift Fur Kristallographie*, 220:567-570.
- Delley B, 1986. Calculated electron distribution for tetrafluoroterephthalonitrile (TFT). *Chemical Physics*, 110: 329-338.  
[http://dx.doi.org/10.1016/0301-0104\(86\)87089-6](http://dx.doi.org/10.1016/0301-0104(86)87089-6)
- Environmental Protection Agency (EPA), , 2011. National Emission Standards for Hazardous Air Pollutants from Coal-and Oil-fired Electric Utility Steam Generating Units and Standards of Performance for Fossil-Fuel-Fired Electric Utility, Industrial- Commercial-Institutional, and Small Industrial-Commercial- Institutional Steam Generating Units [Online]. Available: <https://www.federalregister.gov/articles/2016/04/06/2016-06563/national-emission-standards-for-hazardous-air-pollutants-from-coal--and-oil-fired-electric-utility>. [Accessed Feb., 15th 2016]
- Enyashin AN, Seifert G, 2012. Density-functional study of  $\text{Li}_x\text{MoS}_2$  intercalates ( $0 \leq x \leq 1$ ). *Computational and Theoretical Chemistry*, 999:13-20.  
<http://dx.doi.org/10.1016/j.comptc.2012.08.005>
- Galbreath KC, Zygarlicke CJ, 1996. Mercury speciation in coal combustion and gasification flue gases. *Environmental Science & Technology*, 30:2421-2426.  
<http://dx.doi.org/10.1021/es950935t>
- Gao G, Jiao Y, Ma F, et al., 2015. Charge mediated semi-conducting-to-metallic phase transition in molybdenum disulfide monolayer and hydrogen evolution reaction in new 1T' phase. *The Journal of Physical Chemistry C*, 119:13124-13128.  
<http://dx.doi.org/10.1021/acs.jpcc.5b04658>
- Gao Y, Zhang Z, Wu J, et al., 2013. A critical review on the heterogeneous catalytic oxidation of elemental mercury in flue gases. *Environmental Science & Technology*, 47:10813-10823.  
<http://dx.doi.org/10.1021/es402495h>
- Goki E, Takeshi F, Hisato Y, et al., 2012. Coherent atomic and electronic heterostructures of single-layer  $\text{MoS}_2$ . *ACS Nano*, 6:7311-7317.  
<http://dx.doi.org/10.1021/nn302422x>
- Hasnip PJ, Refson K, Probert MI, et al., 2014. Density functional theory in the solid state. *Philosophical Transactions of the Royal Society A: Mathematical, Physical and Engineering Sciences*, 372:20130270.  
<http://dx.doi.org/10.1098/rsta.2013.0270>
- Huang Z, Hao G, He C, et al., 2013. Density functional theory study of Fe adatoms adsorbed monolayer and bilayer  $\text{MoS}_2$  sheets. *Journal of Applied Physics*, 114:083706.  
<http://dx.doi.org/10.1063/1.4818952>
- Johansen VC, 2003. Mercury speciation in other combustion sources: a literature review. *Portland Cement Association*, 2578:20.
- Jones DW, 1999. Exposure or absorption and the crucial question of limits for mercury. *Journal of the Canadian Dental Association*, 65(1):42-46.
- Liang S, Wang Y, Cinnirella S, et al., 2015. Atmospheric mercury footprints of nations. *Environmental Science & Technology*, 49:3566-3574.  
<http://dx.doi.org/10.1021/es503977y>
- Lim D, Wilcox J, 2013. Heterogeneous mercury oxidation on Au(111) from first principles. *Environmental Science & Technology*, 47:8515-8522.  
<http://dx.doi.org/10.1021/es400876e>
- Liu D, Chen X, Li D, 2010. Simulation of  $\text{MoS}_2$  crystal structure and the experimental study of thermal decomposition. *Journal of Molecular Structure*, 980:66-71.  
<http://dx.doi.org/10.1016/j.molstruc.2010.06.038>
- Ortmann F, Bechstedt F, Schmidt WG, 2006. Semiempirical van der Waals correction to the density functional description of solids and molecular structures. *Physical Review B*, 73:205101.  
<http://dx.doi.org/10.1103/PhysRevB.73.205101>
- Pfrommer BG, Cote M, Louie SG, et al., 1997. Relaxation of crystals with the quasi-Newton method. *Journal of Computational Physics*, 131:233-240.  
<http://dx.doi.org/10.1006/jcph.1996.5612>
- Praveen A, 2003. Mercury emissions from coal fired power plants. Northeast States for Coordinated Air Use Management.
- Presto AA, Granite EJ, 2006. Survey of catalysts for oxidation of mercury in flue gas. *Environmental Science & Technology*, 40:5601-5609.  
<http://dx.doi.org/10.1021/es060504i>
- Putungan DB, Kuo JL, 2014. Structural and electronic properties of monolayer 1T- $\text{MoS}_2$  phase, and its interaction with water adsorbed on perfect, single S-Vacated and  $\text{MoS}_2$ -unit-vacated surface: density functional theory calculations. *Integrated Ferroelectrics*, 156:93-101.  
<http://dx.doi.org/10.1080/10584587.2014.906790>
- Sato T, Nakai H, 2009. Density functional method including weak interactions: dispersion coefficients based on the local response approximation. *The Journal of chemical physics*, 131:224104.

- <http://dx.doi.org/10.1063/1.3269802>
- UNEP, 2002. Global Mercury Assessment [Online]. Available: <http://www.unep.org> [Accessed Jan., 15th 2016].
- UNEP, 2013a. Final Act of the Conference of Plenipotentiaries on the Minamata Convention on Mercury [Online]. Available: [www.mercuryconvention.org/](http://www.mercuryconvention.org/) [Accessed April, 15th 2016]. Japan.
- UNEP, 2013b. Global Mercury Assessment 2013: sources, emissions, releases, and environmental transport [Online]. Available: <http://www.unep.org> [Accessed April, 15th 2016].
- UNEP, 2013c. The Minamata Convention on Mercury [Online]. Available: <http://www.mercuryconvention.org/Convention/tabid/3426/> [Accessed April, 15th 2016].
- Vanderbilt D, 1990. Soft self-consistent pseudopotentials in a generalized eigenvalue formalism. *Physical Review B*, 41:7892-7895.  
<http://dx.doi.org/10.1103/PhysRevB.41.7892>
- Wypych F, Schollhorn R, 1992. 1T-MoS<sub>2</sub>, a new metallic modification of molybdenum disulfide. *Journal of the Chemical Society, Chemical Communications*, (19):1386-1388.  
<http://dx.doi.org/10.1039/C39920001386>
- Wypych F, Weber T, Prins R, 1998. Scanning tunneling microscopic investigation of 1T-MoS<sub>2</sub>. *Chemistry of Materials*, 10:723-727.  
<http://dx.doi.org/10.1021/cm970402e>
- Yin Z, Li H, Li H, *et al.*, 2011. Single-layer MoS<sub>2</sub> phototransistors. *ACS Nano*, 6:74-80.  
<http://dx.doi.org/10.1021/nn2024557>
- Zhao H, Yang G, Gao X, *et al.*, 2016. Hg(0) capture over CoMoS/γ-Al<sub>2</sub>O<sub>3</sub> with MoS<sub>2</sub> nanosheets at low temperatures. *Environmental Science & Technology*, 50:1056-1064.  
<http://dx.doi.org/10.1021/acs.est.5b04278>

的硫 (S) 和钼 (Mo) 原子的影响。吸附的汞 (Hg) 原子在 1T-MoS<sub>2</sub> 的 T<sub>10</sub> 位置上会被氧化, 其吸附能为 -1.091 eV。从局部态密度 (PDOS) 分析来看, Hg 原子和 1T-MoS<sub>2</sub> 表面之间的相互作用是由汞 (Hg) 原子的 d 轨道的与硫 (S) 原子的 p 轨道和钼 (Mo) 原子的 d 轨道重叠所致。

## 中文概要

由于零价态汞 (Hg) 对人体健康和生态环境的负面影响, 它已逐渐成为全球关注的焦点。对 2H-MoS<sub>2</sub> (棱镜结构二硫化钼) 脱除零价汞 (Hg<sup>0</sup>) 的研究已经有了很多工作进展。然而, 二硫化钼的另一个型态, 1T-MoS<sub>2</sub> (多型结构的二硫化钼) 的除汞机制仍未被探索。因此, 本次研究采用密度泛函理论 (DFT) 分析 Hg<sup>0</sup> 在 1T-MoS<sub>2</sub> 单层上的吸附机理。对 1T-MoS<sub>2</sub> 的不同吸附位置进行了考察。对于不同的吸附构型, 还研究了电子吸附前后的变化, 从而进一步了解吸附过程。研究结果表明, 化学吸附是 Hg 原子与 1T-MoS<sub>2</sub> 单层吸附的主导因素。同时, 在所有可能的吸附位置中, T<sub>10</sub> (在钼原子上方) 的位置是最强烈的吸附构型。汞 (Hg) 原子在 1T-MoS<sub>2</sub> 单层上的吸附受邻近